Journal of Machine Engineering, 2026, Vol. 26
ISSN 1895-7595 (Print) ISSN 2391-8071 (Online)

Received*: 28 January 2026* / Accepted: *21 April 2026* / Published online: *29 April 2026*

on-machine scanning,
scanning probe,
dynamic error,
high-speed measurement

Katarzyna MATYS-POPIELSKA[1,2*], René MAYER[1],
Adam WOŹNIAK[2], Rachid GUIASSA[3]

HIGH-SPEED ON-MACHINE METROLOGY: THE IMPACT OF OPERATIONAL PARAMETERS AND WORKPIECE GEOMETRY ON CONTACT SCANNING ACCURACY

Contact coordinate measuring systems determine the dimensions and forms of complex geometries. In the context of Industry 4.0, measurement integration into the manufacturing process, such as a machine tool, is sought. On-machine measurement (OMM) may enhance productivity and reduce costs, but it also presents challenges, including the presence of coolant and contaminants, as well as dynamic errors that impact measurement. The influence of scanning speed and sense, as well as the size and type of the measured ring gauges, on measurement is experimentally investigated based on bidirectional scans of five reference ring gauges at three speeds between 2116 mm/min and 15240 mm/min. The actual measurement deviations from the nominal value were isolated by subtracting the first harmonic from the raw machine and probe readings. The peak-to-peak values and root mean square (RMS) values of probe readings were used to assess the results. The peak-to-peak and RMS values increase as the speed and diameter of the ring increase. In the case of high scanning speed, for example, the RMS value is 0.126 mm, and for low scanning speed, the RMS value is 0.062 mm. The non-parametric Kruskal-Wallis test shows a significant impact of scanning speed (p = 7.75e-9) and ring size (p = 9.31e-4) on the magnitude of error.

1. INTRODUCTION

Contact coordinate measuring systems are essential to ensure the dimensions and forms quality of parts. Initially, this was the domain of coordinate measuring machines (CMM), but in the era of Industry 4.0, the objective is to improve efficiency and reduce production costs [1, 2] in part through the integration of metrological functions within manufacturing processes, such as, for example, the integration of contact probes on machine tools [3]. Scanning probes enable the continuous collection of large quantities of points on the surface of a component, rather than point-by-point measurement, providing rich metrological data in a short time (e.g., 1000 points per second for the Renishaw OSP60 probe) and reducing the

[1] Department of Mechanical Engineering, École Polytechnique de Montréal, Canada
[2] Faculty of Mechatronics, Warsaw University of Technology, Poland
[3] Pratt and Whitney Canada, Canada
[*] E-mail: katarzyna.matys.dokt@pw.edu.pl
https://doi.org/10.36897/jme/220900

risk of missing surface defects. However, as scanning speeds increase, a thorough analysis of the factors influencing dynamic error is essential for designing measurement processes, estimating measurement uncertainty, and potentially compensating for measurement bias in high-speed measurements.

Various experimental methods are used to determine the characteristics of probe dynamic errors. Probes designed and built by researchers or those with a well-known design can be tested using simulation. Yu et al. [4] modelled a probe and performed a finite element analysis (FEA) to determine its natural frequency. Based on theoretical analysis and actual signal data from self-developed probe, Shen et al. [5] proposed a model based on the delay in the response of a second-order system subjected to ramp excitation. Zheng et al. [6] designed a probe's structure and then optimized five parameters to achieve high sensitivity and minimize the resonance amplitude. They also used FEA to determine the natural frequency of the probe, and in [7] proposed a compensation method based on previously determined parameters. In [8], an autoregressive moving average model with a long short-term memory network is used to compensate for dynamic errors; in this case, the self-developed probe was tested on a test stand with generated motion, but no dynamic errors and compensation were demonstrated on actual measurement data. Jiang et al. [9] proposed a simple probe construction, for which they determined the dynamic parameters using a one-dimensional micro-moving stage (P-620.1 from Physic Instrument GmbH) and an eddy current sensor (ECS) as a reference. They developed a compensation algorithm based on Bayesian inversion for dynamic compensation. However, it is not possible to use these methods directly to determine the dynamic parameters of commercial systems whose internal structure is unknown. Lv et al. [10] analyse the dynamic behaviour of a self-developed probe during approaching, stabilization, and retraction stages, but use this analysis solely to optimize point measurements.

In the case of an unknown internal structure, Lu et al. [11] determined system parameters for one axis indirectly by measuring the spring stiffness, damping coefficient, and mass through analysis of the response to a step excitation. They calculated the dynamic parameters based on the proposed model and test results. The results were presented for a single radius of the base circle, with four speeds, the highest of which was only 516 mm/min, which is quite slow for modern probes and machines [12]. Meanwhile, Woźniak and Krajewski [13] proposed a method for testing the dynamic errors of a probe. They used two gauge surfaces inclined at an angle as a reference surface, which was scanned as an unknown curve. A dynamic reaction was observed at the transition from a flat surface to an inclined surface. However, this solution does not characterize the magnitude of errors under actual measurement conditions and is also limited to speeds below 600 mm/min. Furthermore, it cannot be used on a machine tool, as it operates in open-loop mode and, therefore, always with a predefined nominal geometry.

In the manufacturing process, dynamic errors of the machine and tool may have a significant impact [14], and together with machine tool kinematic errors, must be known and possibly avoided or compensated to ensure accurate part production [15, 16]. Similarly, in on-machine measurement, the dynamic error characteristic of the probe is as relevant as the error characteristics of the machine tool.

Current research focuses on measurements taken at significantly lower scanning speeds, presenting methods for compensating dynamic error without analysing its magnitude or how it varies with respect to measurement parameters other than speed, relying mainly on the capabilities of self-developed probes.

The purpose of this article is: (1) to analyse the magnitude of dynamic errors based on the scans of ring gauges on a machine tool in relation to the speed and sense of scanning and the size and type of the gauges; (2) to analyse the frequency contents of dynamic errors, and (3) to suggest possible source for the errors of the probe.

2. EXPERIMENTAL PROCEDURE

2.1. EXPERIMENTAL SETUP

Five ring gauges were measured, three with outer nominal diameters (OD) of 25.4 mm, 152.4 mm, and 216 mm, and two with inner nominal diameters (ID) of 50.8 mm and 177.8 mm. For each diameter, the measurement was performed at three speeds: v_1, $v_2 = 0.7v_1$, and $v_3 = 0.3v_1$. The maximum speed for the two smallest rings was lower than that for the others, due to limitations of the machine tool in maintaining a sufficiently precise circular path, with the increasing acceleration when the diameter decreases. This limits the ability to compare results across different ring sizes, while still allowing for comparisons of results in terms of scanning direction or speed within a single diameter. For each speed, two measurements were taken in a clockwise sense (CW) and two in a counterclockwise sense (CCW). The test parameters are presented in Table 1.

Table 1. Parameters of the tests

Ring identifier	Nominal diameter [mm]	Actual diameter [mm]	Type of diameter	Scanning speeds [mm/min]			Sense of the scan	Additional mass on the stylus
				v_1	v_2	v_3		
1	25.4	25.4415	Outer	7055	4938	2116	CCW and CW	no
2	152.4	152.4494	Outer	15240	10668	4572	CCW and CW	no
3	216	215.9327	Outer	15240	10668	4572	CCW and CW	no
4	50.8	50.7045	Inner	9210	6447	2763	CCW and CW	no
5	177.8	177.8116	Inner	15240	10668	4572	CCW and CW	no
1	25.4	25.4415	Outer	7055	4938	2116	CCW and CW	yes

Tests were performed on a five-axis machine tool with a Renishaw OSP60 scanning probe, also known as Renishaw SPRINT, with a 50 mm long stylus and a 4 mm tip diameter (Fig. **1**a).

The OSP60 probe collects points at a constant sampling frequency of 1000 Hz. Measurement always takes place in an open loop, which means that the machine tool does not alter its path according to the probe readings, and so only a nominally known geometry can be scanned. To ensure contact between the probe and the surface, the measurement is performed with an initial nominal deflection, defined as the engagement of the probe tip with

the nominal surface, typically 0.625 mm. This allows for the measurement of geometries that deviate by ±0.5 mm from nominal (the calibrated probe deflection range is 0.125 mm to 1.125 mm).

An additional measurement of Ring 1 at velocity v_1 was performed with additional mass added to the stylus, as shown in Fig. 1b).

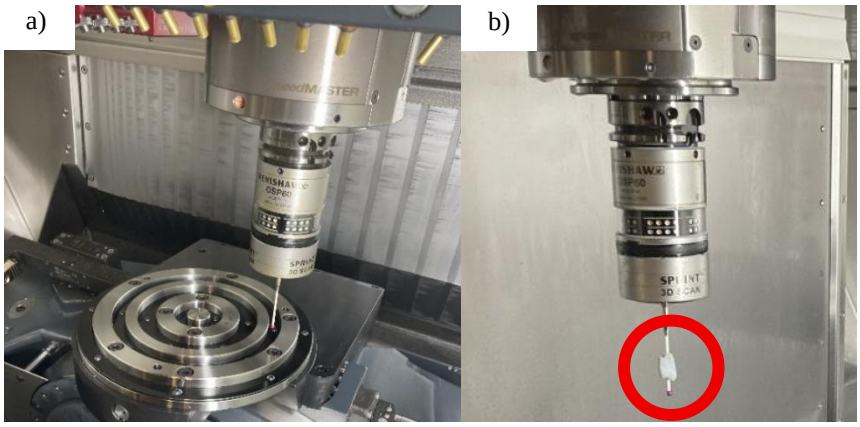

Fig. 1. a) Experimental setup used in the test, b) setup with additional mass on the stylus

2.1. EXPERIMENTAL DATA

The raw measurement data contains the position of the machine tool (probe position in space) and the probe reading separately in each sense. The probe reading is also referred to as the stylus deflection, given an ideal scenario. The raw data also include the measurement result, $M_r = (m_{rx}, m_{ry}, m_{rz})$, which is the sum of the raw machine axis position readings, $A_r = (a_{rx}, a_{ry}, a_{rz})$, and the raw stylus deflection readings or raw probe readings, $P_r = (p_{rx}, p_{ry}, p_{rz})$, as follows:

$$\mathrm{M_r} = \mathrm{A_r} + \mathrm{P_r} \tag{1}$$

The results of the measurement sequence are presented in Fig. 2. In this study, only the coordinates in the plane of the ring are analysed, i.e., the x and y coordinates, as the z coordinate is not considered in the evaluation of the diameter dimension and form error. The probe readings are expressed in the probe reference frame and projected in a frame co-parallel with the machine tool frame defined by its moving linear axes. The probe is not rotating, but only translating during the tests, so that the coordinate transformation is assumed constant. This is done automatically by Renishaw's Productivity+ software, which allows designing measurements and generating reports with probe readings, machine axis position readings, and measurement results.

Fig. 3 shows the scanning measurement of the ring, along with the setting parameters, including the radius of the scanned ring (R_{ring}) and the radius of the tip (r_{tip}). During scanning, the ring mounted on the table remains stationary within the machine tool space; the scan is performed by translating the probe along the x and y axes. This movement is shown in measurement results (Fig. 2).

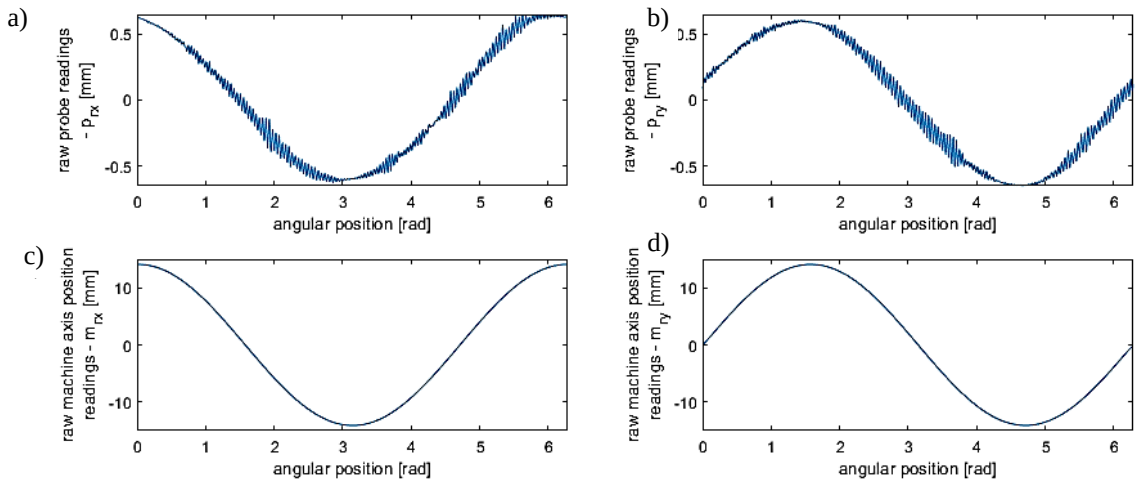

Fig. 2. Measurement of a single circle scan on Ring 1 at speed v_1 in the CCW sense, raw probe readings a) in x-axis -p_{rx}, b) in y-axis - p_{ry}, c) raw machine x-axis position readings -m_{rx}, d) raw machine y-axis position readings -m_{ry}

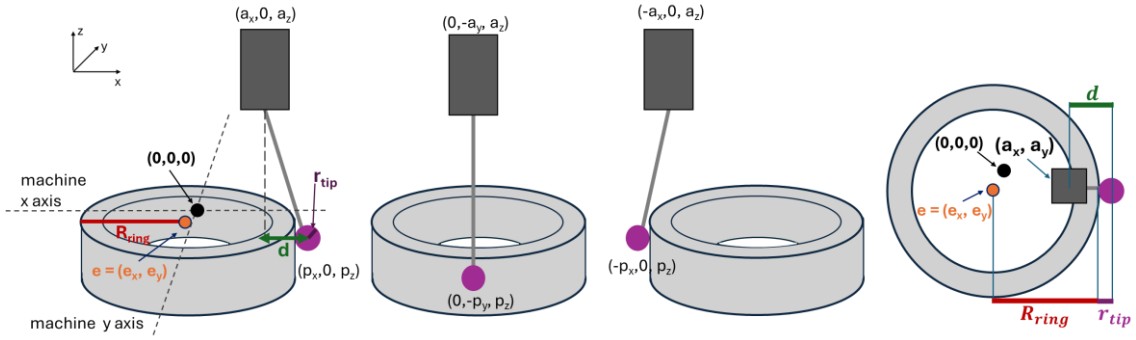

Fig. 3. Nominal movement of the machine axis and probe during scanning of a ring with radius R_{ring} with a stylus tip radius r_{tip} and nominal deflection d, when the gauge ring is placed with eccentricity $e = (e_x, e_y)$ relative to the predetermined center of the machine path

The measurement results contain information about the set up, which is visible as a sinusoidal signal with the lowest frequency also called as a first harmonic. The nominal first harmonic of the machine axis position readings $N_m = (N_{mx}, N_{my})$ depends on the nominal radius of the scanned ring R_{ring} and of the stylus tip r_{tip}, and the nominal deflection d of the stylus tip relative to the probe body. The first harmonic of the probe readings $N_p = (N_{px}, N_{py})$ contains, minimally, information about the nominal deflection d and eccentricity $e = (e_x, e_y)$ of the ring centre relative to the machine tool circular path. N_m and N_p values for the Ring 1 calculated based on Equations **Błąd! Nie można odnaleźć źródła odwołania.** to **Błąd! Nie można odnaleźć źródła odwołania.** are shown in Fig. **4**.

$$N_{mx} = \left(R_{ring} + r_{tip} - d\right) cos\left(atan2\left(a_y, a_y\right)\right) \tag{2}$$

$$N_{my} = \left(R_{ring} + r_{tip} - d\right) sin\left(atan2\left(a_y, a_y\right)\right) \tag{3}$$

$$N_{px} = d\, cos\left(atan2\left(a_y, a_y\right)\right) + e_x \tag{4}$$

$$N_{py} = d \sin\left(atan2\left(a_y, a_y\right)\right) + e_y \tag{5}$$

All this nominal information remains the same for a given configuration and is related only to the measurement settings, not to the actual measurement itself, which may be affected

by a variety of machine, probe, and ring gauge factors.

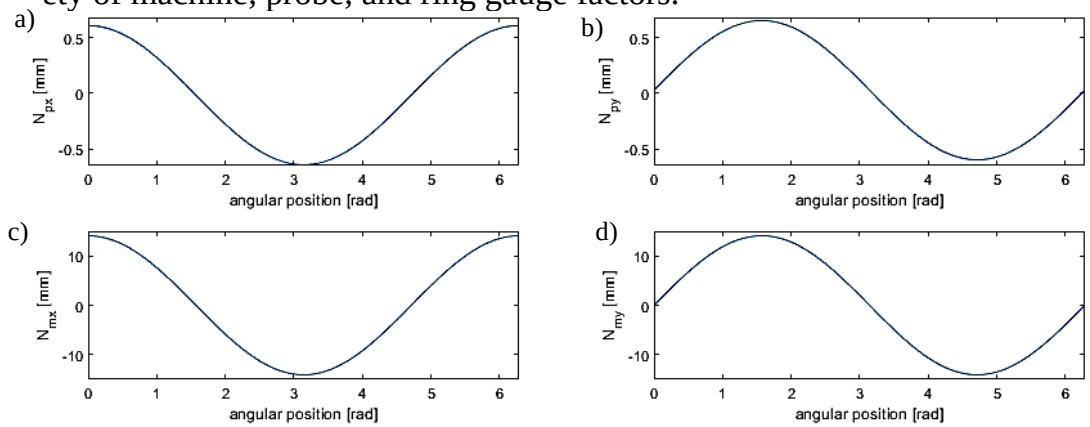

Fig. 4. Nominal first harmonic for a single circle scan on Ring 1 of a) probe readings in x, b) probe readings in y, c) machine x-axis position readings, and d) machine y-axis position readings

Therefore, to make the departure from nominally expected results more visible, the first harmonic of the machine axis position N_m was calculated according to Equations **Błąd! Nie można odnaleźć źródła odwołania.** and **Błąd! Nie można odnaleźć źródła odwołania.**, as all the parameters are previously known, and subtracted from the raw machine axis position readings A_r as follows:

$$A = A_r - N_m \tag{6}$$

For the probe readings, the value of the eccentricity is a setup parameter which is not known prior to the measurement. Hence, the first harmonic was calculated as equation **Błąd! Nie można odnaleźć źródła odwołania.**, and the coefficients: a_0, a_c, and a_s were calculated as an optimal fit $\hat{x}$ in the least squares sense, performed by the operator $A\backslash x$, where A is the constant, cosine, and sine signals, and x is the signal to which the harmonic is adjusted.

$$\hat{x} = a_0 + a_c \cos\left(\frac{2\pi t}{N}\right) + a_s \sin\left(\frac{2\pi t}{N}\right) \tag{7}$$

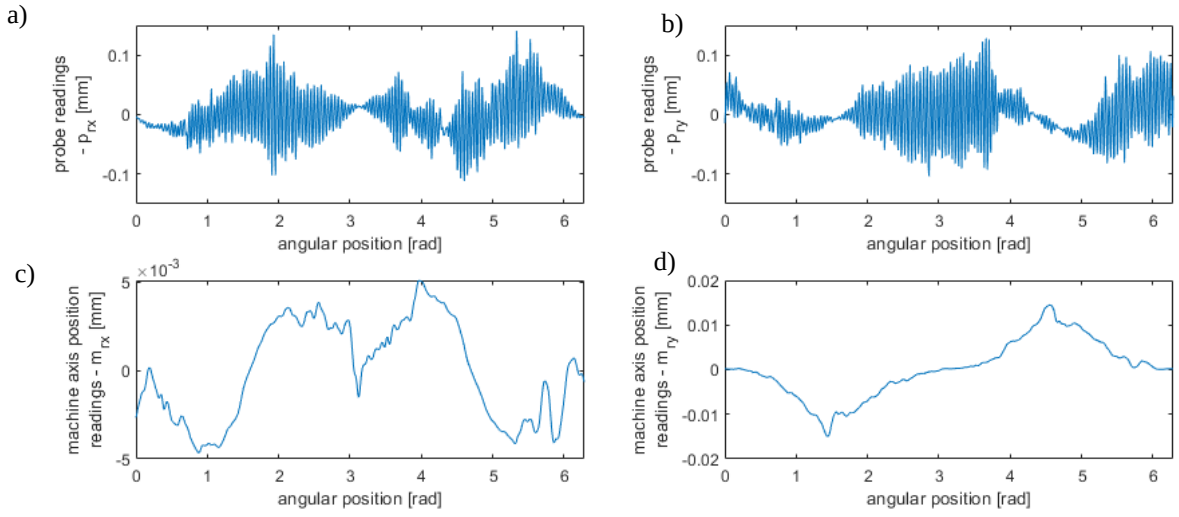

Fig. 5. Scanning measurement of a single circle on Ring 1 at speed v_1 in the CCW sense, a) probe readings in *x*, b) probe readings in *y*, c) machine x-axis position readings, d) machine y-axis position readings without the first harmonic

This first harmonic of probe readings was subtracted from the raw probe readings P_r as follows:

$$P = P_r - N_p \tag{8}$$

The probe readings with the first harmonic removed, in short probe readings *P*, and the machine axis position readings with the first harmonic subtracted, in short machine axis position readings *A*, are shown in **Fig. 5**.

3. RESULTS AND DISCUSSION

3.1. RESULTS

The peak-to-peak and RMS values for probe readings for all test configurations and for two repetitions are presented in Table 2. Based on these values, a statistical analysis was performed.

To perform a one-way analysis of variance (ANOVA) three assumptions must be met: the dependent variable data (peak-to-peak values and RMS) in each group (scanning speed, sense of the scan, size of the ring) must be normally distributed, the variance should be homogeneous, i.e., the variances of the dependent variable should be similar in all groups, and the observations in each group must be independent. The Shapiro-Wilk test was used to check whether the peak-to-peak and RMS values for the p_x and p_y came from a normal distribution.

The *p*-values were 0.003, 0.0002, 0.0002, and 0.0002, which allowed us to reject the hypothesis that the data came from a normal distribution; therefore, the first assumption is not fulfilled. In addition, for each factor: scanning speed and sense, ring size and type, the Levene's test was performed to check the homogeneity of variance. The results of this test are presented in Table 3.

In groups differing in the sense of scan in both axes, and in the group varying in the type of ring for the y-axis, the *p*-value is greater than 0.05, which means that the assumption of homogeneity of variance is satisfied only in these groups. In the other groups, this assumption is not fulfilled. Therefore, it is not possible to perform an ANOVA analysis. It was decided to use the non-parametric Kruskal-Wallis test [17]. The test compares separate factors, not configurations as a whole. Therefore, although there are only 2 repetitions in each configuration, a total of 60 observations are compared: 20 samples for each speed, 30 for each direction, and 12 for each ring size. Since the Kruskal-Wallis test is based on comparing ranks across the entire dataset, the test can detect if the tested factor consistently shifts the results toward higher ranks, regardless of the variation of other factors within a group. Furthermore, as these measurements are deterministic in nature, probe errors will not be random phenomena.

In each of the tests, the null hypothesis was set that there are no significant differences between the peak-to-peak values for different factors. The test results are presented in Table 4.

Table 2. Peak-to-peak and RMS values of probe readings for every test configuration, repeated twice

Ring	Scanning speeds [mm/min]	Sense of the scan	Peak-to-peak of p_x [mm]		Peak-to-peak of p_y [mm]		RMS of p_x [mm]		RMS of p_y [mm]	
Ring 1	v_1	CCW	0.253	0.277	0.232	0.203	0.038	0.043	0.040	0.036
Ring 1	v_2	CCW	0.195	0.219	0.223	0.200	0.031	0.035	0.035	0.037
Ring 1	v_3	CCW	0.149	0.144	0.139	0.141	0.022	0.022	0.021	0.021
Ring 1	v_1	CW	0.264	0.236	0.285	0.258	0.039	0.043	0.048	0.050
Ring 1	v_2	CW	0.209	0.180	0.193	0.183	0.034	0.034	0.033	0.033
Ring 1	v_3	CW	0.144	0.116	0.141	0.146	0.021	0.020	0.021	0.021
Ring 2	v_1	CCW	0.493	0.490	0.490	0.408	0.093	0.091	0.094	0.089
Ring 2	v_2	CCW	0.369	0.374	0.399	0.381	0.058	0.053	0.065	0.062
Ring 2	v_3	CCW	0.232	0.212	0.235	0.210	0.031	0.030	0.030	0.030
Ring 2	v_1	CW	0.469	0.424	0.487	0.532	0.087	0.080	0.089	0.089
Ring 2	v_2	CW	0.344	0.326	0.369	0.315	0.054	0.048	0.050	0.044
Ring 2	v_3	CW	0.207	0.208	0.209	0.191	0.032	0.031	0.030	0.030
Ring 3	v_1	CCW	0.570	0.523	0.642	0.569	0.114	0.107	0.118	0.107
Ring 3	v_2	CCW	0.416	0.402	0.391	0.388	0.078	0.073	0.077	0.074
Ring 3	v_3	CCW	0.229	0.223	0.200	0.210	0.034	0.033	0.034	0.033
Ring 3	v_1	CW	0.553	0.550	0.643	0.627	0.117	0.111	0.118	0.114
Ring 3	v_2	CW	0.389	0.388	0.422	0.429	0.078	0.077	0.077	0.078
Ring 3	v_1	CCW	0.205	0.198	0.212	0.207	0.033	0.032	0.034	0.034
Ring 4	v_1	CCW	0.311	0.309	0.305	0.293	0.063	0.063	0.059	0.061
Ring 4	v_2	CCW	0.230	0.233	0.223	0.216	0.044	0.043	0.042	0.042
Ring 4	v_3	CCW	0.153	0.149	0.164	0.145	0.023	0.023	0.024	0.024
Ring 4	v_1	CW	0.328	0.316	0.307	0.330	0.065	0.065	0.065	0.061
Ring 4	v_2	CW	0.227	0.253	0.227	0.231	0.045	0.043	0.044	0.041
Ring 4	v_3	CW	0.165	0.161	0.142	0.138	0.023	0.023	0.023	0.023
Ring 5	v_1	CCW	0.393	0.354	0.528	0.449	0.073	0.061	0.096	0.069
Ring 5	v_2	CCW	0.336	0.292	0.410	0.423	0.052	0.050	0.062	0.067
Ring 5	v_3	CCW	0.211	0.199	0.247	0.210	0.030	0.028	0.029	0.028
Ring 5	v_1	CW	0.433	0.389	0.500	0.489	0.077	0.063	0.092	0.084
Ring 5	v_2	CW	0.343	0.312	0.376	0.403	0.059	0.051	0.061	0.063
Ring 5	v_3	CW	0.205	0.194	0.218	0.215	0.029	0.027	0.029	0.028

Table 3. Variance check with Levene's test of peak-to-peak values of probe readings

Factor	Peak-to-peak of p_x		Peak-to-peak of p_y		RMS of p_x		RMS of p_y	
	Levene's test	*p*-value	Levene's test	*p*-value	Levene's test	*p*-value	Levene's test	*p*-value
Scanning speed	15.230	0.000	23.762	0.000	14.596	0.000	26.831	0.000
Scanning sense	0.008	0.931	0.063	0.803	0.007	0.934	0.001	0.973
Ring size	3.736	0.009	5.804	0.001	4.970	0.002	4.609	0.003
Ring type	10.168	0.002	2.645	0.109	9.317	0.003	4.424	0.040

Table 4. Kruskal-Wallis test for the peak-to-peak values of probe readings for different factors

Factor	Peak-to-peak of p_x		Peak-to-peak of p_y		RMS of p_x		RMS of p_y	
	test statistic	*p*-value	test statistic	*p*-value	test statistic	*p*-value	test statistic	*p*-value

Scanning speed	37.352	7.75e-9	33.080	6.56e-8	41.983	7.65e-10	41.826	8.27e-10
Scanning sense	0.116	0.734	0.0002	0.988	0.0002	0.988	0.003	0.953
Ring size	18.626	9.31e-4	21.228	2.85e-4	14.876	0.005	14.843	0.005
Ring type	0.740	0.390	0.008	0.928	0.312	0.577	0.233	0.629

3.1.1. EFFECT OF SCANNING SPEED

Fig. **6** shows probe readings for scans of Ring 1 (Fig. **6**a), Ring 3 (Fig. **6**b), and Ring 5 (Fig. **6**c) in the CCW sense and each at three speeds v_1, v_2, and v_3. For different speeds, the probe readings differ in amplitude, both in terms of peak values (Fig. **7**) and root mean square (RMS) values (Fig. **8**).

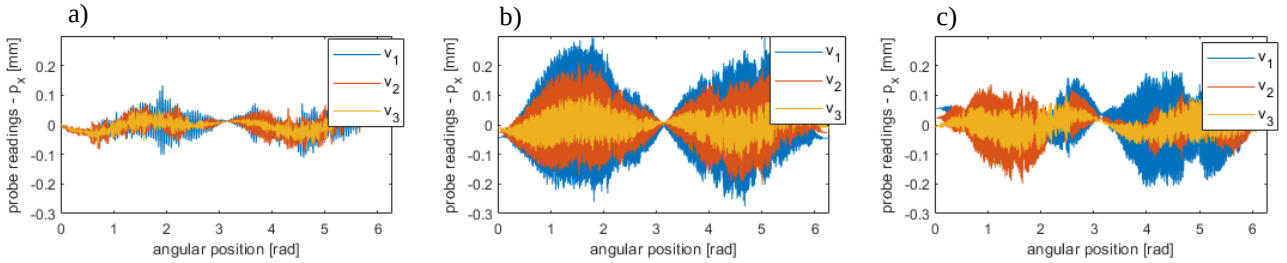

Fig. 6. Comparison of probe readings for scans of a) Ring 1, b) Ring 3, and c) Ring 5 in the CCW sense at three speeds v_1, v_2, v_3 for the x-axis

For Ring 1 on the x-axis, the peak-to-peak value (Fig. **7**a) for the highest speed is 0.253 mm and for the lowest speed 0.149 mm, while for Ring 3 (Fig. **7**b) it is 0.570 mm and 0.229 mm, respectively. Similarly, RMS values increase with higher speed as shown in Fig. **8**. for Ring 1 on the x-axis (Fig. **8**a), for v_1, RMS is 0.066 mm, and for v_3, RMS is 0.057 mm and for Ring 3 on the x-axis (Fig. **8**c), for v_1, RMS is 0.126 mm, and for v_3, RMS is 0.062 mm. This indicates that an increase in speed results in higher amplitude of the high frequencies contents in the probe readings.

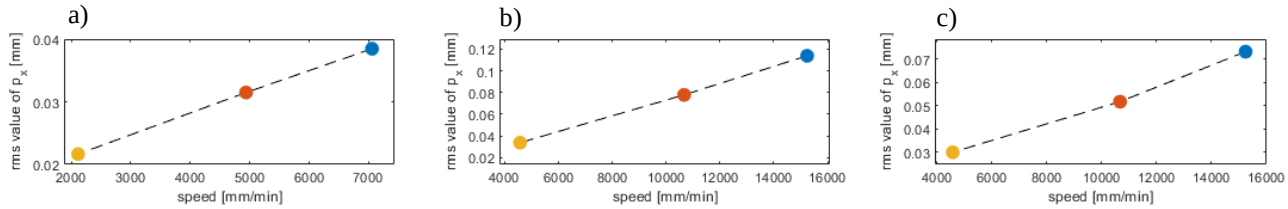

Fig. 7. Peak-to-peak values of probe readings for scans of a) Ring 1, b) Ring 3, and c) Ring 5 in the CCW sense at three speeds v_1, v_2, v_3 for the x-axis

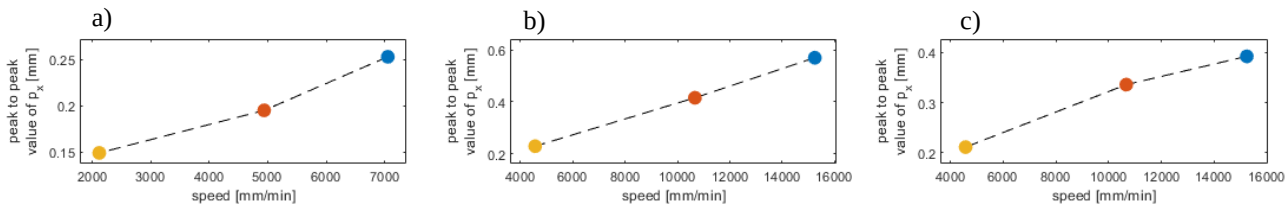

Fig. 8. RMS values of probe readings for scans of a) Ring 1, b) Ring 3, and c) Ring 5 in the CCW sense at three speeds v_1, v_2, v_3 for the x-axis

The Kruskal-Wallis test results are consistent for both axes and both peak-to-peak and RMS values. For different scanning speeds, the *p*-value is 7.75e-9 for peak-to-peak of p_x, 6.56e-8 for peak-to-peak of p_y, 7.65e-10 for RMS of p_x, and 8.27e-10 for RMS of p_y, which is less than 0.05 in every case.

3.1.2. EFFECT OF RING SIZE AND TYPE

Fig. **9** shows probe readings for scans of Ring 2 and Ring 3 (Fig. **9**a), and all rings (Fig. **9**b) in the CCW sense at speed v_1. For rings of different sizes, a slightly different probe response is observed when scanning at maximum speed v_1.

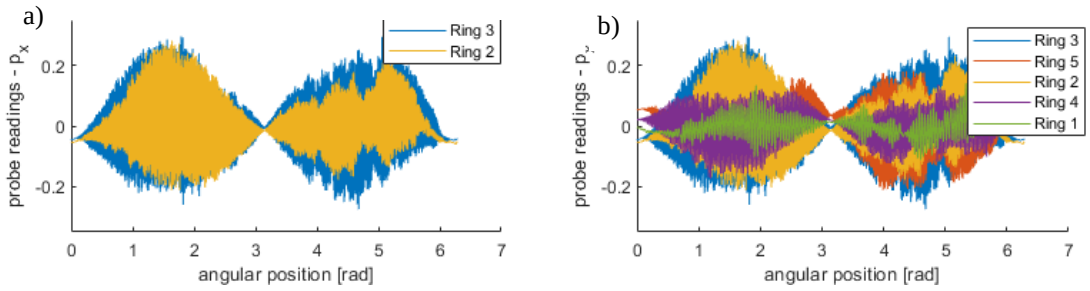

Fig. 9. Comparison of probe reading scans for different ring sizes in the CCW sense at v_1, a) outer rings: Ring 2, and Ring 3, b) all rings sorted by size for the x-axis

When comparing probe readings where only the radius of the scanned ring changes (Fig. **9**a), a noticeable difference in signal amplitude is also observed. The peak-to-peak value and RMS of probe readings (Fig. **10**) are greater for larger rings.

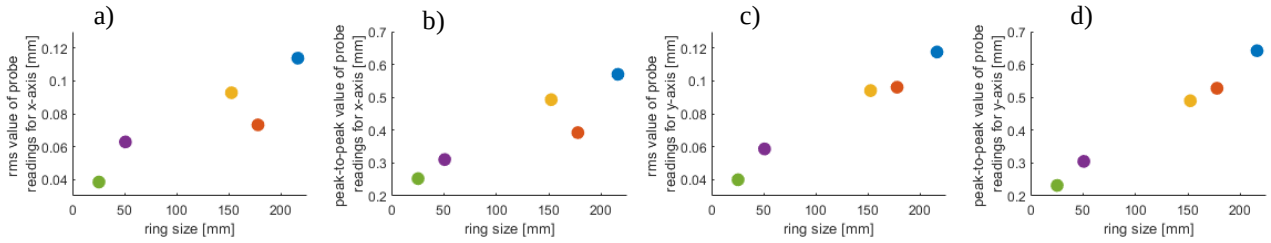

Fig. 10. RMS values of probe readings for scans for a) the x-axis, c) the y-axis, and peak-to-peak values for b) the x-axis, d) the y-axis Rings 1- 5 in the CCW sense at three speeds v_1

For Ring 2, the peak-to-peak value of probe readings is 0.493 mm, and the RMS is 0.110 mm; for Ring 3, it equals 0.570 mm and 0.126 mm, respectively. For all rings, the values for subsequent rings are: 0.253 mm, 0.493 mm, 0.570 mm, 0.311 mm, and 0.393 mm. For different diameters of the scanned ring and ring type, the *p*-value is 9.31e-4 and 0.390 for peak-to-peak of p_x, 2.85e-4 and 0.928 for peak-to-peak of p_y, 0.005 and 0.577 for RMS of p_x, and 0.005 and 0.629, respectively, for RMS of p_y, which is less than 0.05 for different diameters, but greater for ring type.

3.1.3. EFFECT OF SCANNING SENSE

The data for different scan senses are shown in Fig. **11**. It can be seen that the waveforms are similar but not identical. However, there is no statistical difference between peak-to-peak values of probe readings for CW and CCW scans.

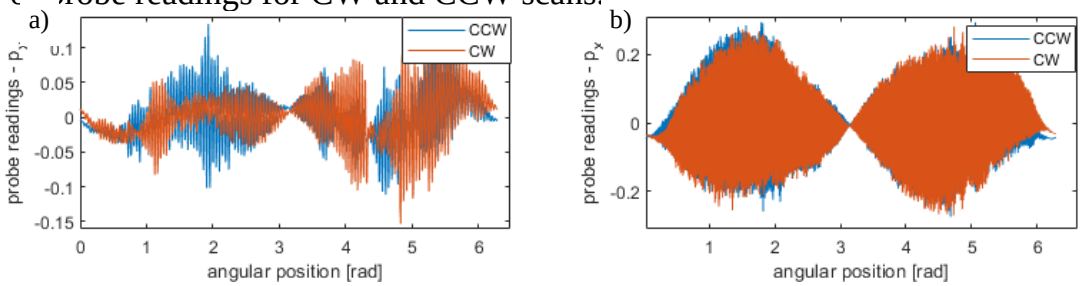

Fig. 11. Comparison of probe readings for scans in both senses for a) Ring 1 and b) Ring 3 with scanning speed v_1 for the x-axis

For the scan sense, the *p*-value for peak-to-peak of p_x is 0.734, for peak-to-peak of p_y is 0.988, for RMS of p_x is 0.988, for RMS of p_y is 0.953, which is greater than 0.05.

3.2. DISCUSSION

The results from scans with three speeds indicate that an increase in speed results in higher amplitude of the high frequency contents in the probe readings. Kruskal-Wallis test confirms that there is a statistically significant difference in peak-to-peak and RMS of probe readings for scanning speed.

The comparison of different sizes of rings for Ring 2 and Ring 3, where the only difference is the ring size (Fig. **9**a), suggests that the size of the ring affects measurement results. When comparing all ring sizes and ring types, it should be noted that more than one parameter has changed. Graphical results suggest that only the ring's size, not its type (outer or inner), affects the measurement results. This is further supported by the statistical analysis and *p*-values greater than 0.05 for ring type, suggesting that there is no statistically significant difference among the results differing in ring type, and *p*-values less than 0.05 for ring size, suggesting that ring size is statistically significant. However, as this hypothesis is likely, it cannot be confirmed, as we do not have a ring with the same diameter but of a different type, and not all scans were performed at the same speed.

As for the scanning sense, as not all of the results are identical, at the 95.0% confidence level, there is no statistically significant difference among the results differing in the sense of the scan.

The increase in errors at higher speeds may be caused by an increase in centrifugal force, which results in greater excitation of the probe's natural frequency. To further investigate the matter, the probe's signal frequency was analysed.

3.3. FREQUENCY ANALYSIS

In order to analyse the nature of the changes observed in the data, an FFT analysis was performed. Sample frequency graphs are shown in Fig. 12. Figure 12a, left, shows the frequency-amplitude plot for the probe readings of Ring 1 at speed v_1 in the CCW sense scan, covering the maximum possible frequency range from 0 to 500 Hz according to the Nyquist criterion. The spectrum shows a distinct group of peaks in the range of 170–195 Hz, with an amplitude close to 0.024 mm. Comparing all frequency-amplitude graphs, regardless of the speed, scanning sense, and size of the ring, the frequency content of the probe readings for different scan configurations is similar, however the graphs differ in amplitude depending on the test parameters.

As scanning speeds and ring diameter increase, higher frequency amplitude in the range of 170–195 Hz is observed, similar to the higher peak-to-peak value observed in Fig. 7 and Fig. 10b and d. The effect of scanning speed on CMMs has been examined both in terms of roundness and diameter variation [18], as well as in terms of the results themselves, including the amplitude of oscillation of the response at some resonance frequency [6]. In both articles, an increase in dynamic variations at higher speeds was observed, although the studies were performed at speeds below 360 mm/min, which is a fraction of the speeds used in the present study.

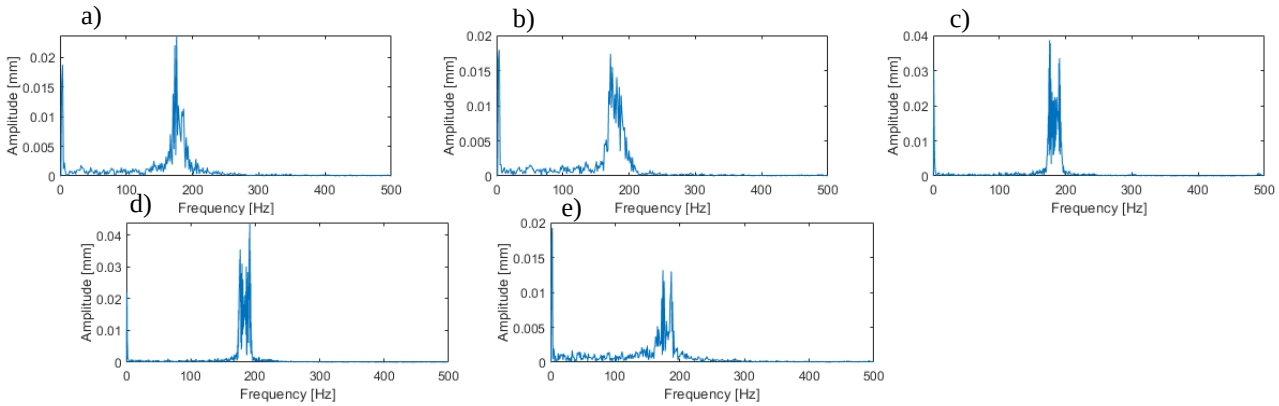

Fig. 12. Frequency-amplitude characteristic of probe readings after removing the first harmonic for five configurations: a) Ring 1 at speed v_1 in the CCW sense, b) Ring 1 at speed v_1 in the CW sense, c) Ring 2 with velocity v_1 in the CCW sense, d) Ring 3 with velocity v_1 in the CCW sense, e) Ring 1 with velocity v_2 in the CCW sense for the x-axis

When changing the measurement sense, as in the cases of peak-to-peak and RMS values, the amplitude of the frequency signal remains at the same level. This is another indication that the scan sense does not affect the measurement result.

Fig. **13** shows the frequency-amplitude characteristic of machine axis position readings. Fig. **13**a shows the entire graph, which displays a low frequency of 1.46 Hz corresponding to nominal movement. In order to show other frequencies with lower amplitudes, the graph has been zoomed in, as shown in Fig. **13**b. Additional frequencies in the range of 0–50 Hz are visible.

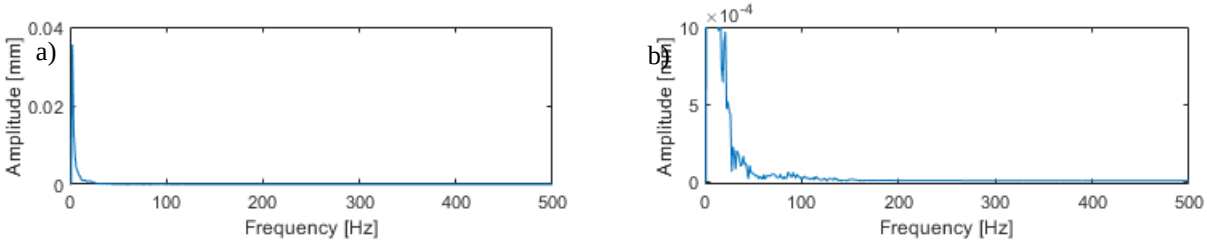

Fig. 13. a) Frequency-amplitude characteristic of machine axis position readings when scanning Ring 1 at speed v_1 in the CCW sense, b) zoom for higher frequencies, for the x-axis

The frequency range observed in the probe readings signal (Fig. **12**) is not present in the signal from the machine tool (Fig. **13**), which suggests that this frequency does not originate from the machine. Furthermore, in the case of the main structure of the machine, due to its high mass, its resonance frequency should not exceed a few dozen hertz [15]. It also rules out the electrical system as the source, as in that case, it should be close to 60 Hz. A possible source of this frequency may be an external vibration source with a constant frequency, which is transmitted to the measuring element, or it may be coming from the probe-stylus system. To test this hypothesis, another scanning measurement of Ring 1 was also performed at speed v_1 in the CCW sense, but with an added mass to the stylus Fig. **1**b). To determine whether the frequency originates from the probe, it is essential to change the mass of the system, but knowing the exact placement of the mass on the stylus is not crucial. Fig. **14** shows a comparison of the frequency content in the probe readings data for the scans without and with the additional mass.

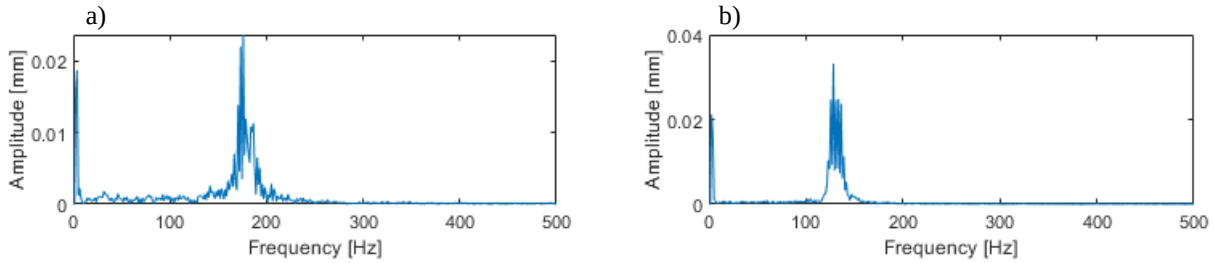

Fig. 14. Frequency contents of the probe readings for Ring 1 at speed v_1 in the CCW sense, a) standard setup, b) with additional mass on the tip, for the x-axis on the left and for the y-axis on the right

After adding the mass, the frequency range decreased from 170–195 Hz down to 115–145 Hz. This result strongly suggests that the source of these vibration frequencies is the probe-stylus system, which may be excited by the movement of the machine axes or the dynamic interaction of the measuring ball with the surface. The suggestion that the frequency in the range 170–195 Hz comes from the probe and stylus assembly is also supported by studies in which researchers examine the dynamic parameters of scanning probes on CMMs [6, 19]. They examine known, custom-designed scanning probes with one or two stylus configurations. Depending on the probe design and the stylus employed, the first-order natural frequency was 142 Hz, 774 Hz, or 942 Hz. This suggests that frequencies between 170 and 195 Hz originate from the natural frequencies of the scanning probe and stylus on a machine tool.

4. CONCLUSIONS AND FUTURE WORK

Based on the scans of five reference rings at five speeds in two senses, the influence of scanning speed and sense, as well as the size and type (ID or OD) of rings, on the probe and machine tool signals was analysed. This research focuses on analysing the dynamic errors of the probe rather than the entire machine, at significantly high measurement speeds (between 2116 mm/min and 15240 mm/min). To make the actual measurement deviations more visible, the first harmonic, due to set up parameters: nominal deflection, eccentricity, ring and tip radius, was calculated and subtracted from the raw machine and probe readings.

Peak-to-peak and RMS values of probe readings were used to assess the results. The highest peak-to-peak and RMS values of 0.570 mm and 0.126 mm, respectively, are obtained for the scan of the ring with the largest diameter (Ring 3) at the highest speed (v_1). The values decrease both with a reduction in the diameter of the scanned ring (for Ring 2, they are 0.493 mm and 0.110 mm) and with a reduction in speed (for v_3, they are 0.229 mm and 0.062 mm). The Kruskal-Wallis test confirmed that the scanning speed and size of the tested ring have a statistically significant impact on the scanning measurement results on the machine tool. Therefore, when planning measurements, the speed should be limited to less than 5,000 mm/min, and even further reduced when scanning extremely large rings. If measurements must be performed at higher speeds, significant dynamic errors must be considered.

A limitation of the study was the lack of the same diameter tests for different types of rings. Although the results suggest that the type of ring does not make a statistically significant difference, this conclusion would need to be confirmed by examining different types of rings with the same diameter.

From the data, dominant frequencies were determined to be a distinct group of peaks in the range of 170–195 Hz. By adding mass to the stylus, which lowered the dominant frequencies to 115–145 Hz, it was shown that the selected frequencies originate from the probe and stylus system.

Future work will use the specific natural frequency and parameters that affect the scanning measurement value to determine the accuracy of the scanning probe in measuring any geometry and serve as a starting point for modelling the scanning measurement process.

REFERENCES

[1] NASRIL et al., 2024, *On-Machine Measurement of Machining Accuracy Based on a Support Vector Regression (SVR) Model for Product Quality Monitoring*, in 2024 IEEE International Conference on Smart Mechatronics (ICSMech), IEEE, 213–218, https://doi.org/10.1109/ICSMech62936.2024.10812316.

[2] WIECZOROWSKI M., TROJANOWSKA J., 2023, *Towards Metrology 4.0 in Dimensional Measurements*, Journal of Machine Engineering, https://doi.org/10.36897/jme/161717.

[3] ARCHENTI A., GAO W., DONMEZ A., SAVIO E., IRINO N., 2024, *Integrated Metrology for Advanced Manufacturing*, CIRP Annals, 73/2, 639–665, 2024, https://doi.org/10.1016/j.cirp.2024.05.003.

[4] YU J., LIN X., YANG Y., CAI J.-H., 2022, *Design and Characteristic Research of Contact Probe for High-Precision 3D Thread-Measuring Machine*, The International Journal of Advanced Manufacturing Technology, 119/3–4, 2235–2245, https://doi.org/10.1007/s00170-021-08345-z.

[5] SHEN Y., et al., 2024, *Dynamic Error Modeling and Compensation of a Scanning Probe on CMM*, IEEE Trans. Instrum. Meas., 73, 1–9, https://doi.org/10.1109/TIM.2024.3476532.

[6] ZHENG W., LIU Z., FU L., GUO J., 2021, *Effective Improvement of Scanning Resonance Through Dynamic Optimization of the Probe*, Measurement, 178, 109438, https://doi.org/10.1016/j.measurement.2021.109438.
[7] ZHENG W., ZHANG G., LI H., YANG X., SHAO W., LIU Z., 2023, *Dynamic Compensation Strategy for Scanning Error of Contact Probe Based on Damping Ratio and Frequency Mapping*, IEEE Sensors Journal, 23/23, 28649–28659, https://doi.org/10.1109/JSEN.2023.3321342.
[8] ZHENG W., ZHANG S., PENG H., TIAN C., ZENG H., SHAO W., 2026, *High-Precision Dynamic Error Compensation for Scanning Probes Via a Hybrid Data-Driven Framework*, Measurement, 261, 120015, https://doi.org/10.1016/j.measurement.2025.120015.
[9] JIANG W.S., CHENG Z.Y., GONG W.C., YU L., LI R.J., HUANG Q.X., 2021, *A Novel Dynamic Compensation Method for a Contact Probe Based on Bayesian Inversion*, Measurement: Journal of the International Measurement Confederation, 186, 1–9, https://doi.org/10.1016/j.measurement.2021.110143.
[10] LV X., SHEN Y., ZHANG X., HUA Z., GUO W., TU D., 2026, *Selection of Measurement Parameters Based on the Dynamic Characteristics of the Scanning Probe*, Measurement, 266, 120501, https://doi.org/10.1016/j.measurement.2026.120501.
[11] LU C., WANG J., ALIMUJIANG A., LI S., HOU Z., 2022, *Dynamics Model of Scanning Probe on GMC*, Measurement, 199, 111472, https://doi.org/10.1016/j.measurement.2022.111472.
[12] SHEN Y., REN J., HUANG N., ZHANG Y., ZHANG X., ZHU L., 2023, *Surface Form Inspection with Contact Coordinate Measurement: A Review*, Int. J. Extrem. Manuf., 5/2, 022006, https://doi.org/10.1088/2631-7990/acc76e.
[13] WOZNIAK A., KRAJEWSKI G., BYSZEWSKI M., 2019, *A New Method for Examining the Dynamic Performance of Coordinate Measuring Machines*, Measurement, 134, 814–819, https://doi.org/10.1016/j.measurement.2018.12.041.
[14] LYU D., LIU Q., LIU H., ZHAO W., 2020, *Dynamic Error of CNC Machine Tools: A State-of-the-Art Review*, The International Journal of Advanced Manufacturing Technology, 106, 5–6, 1869–1891, https://doi.org/10.1007/s00170-019-04732-9.
[15] LIU Q., et al., 2025, *Geometric and Dynamic Error Compensation of Dual-Drive Machine Tool Based on Mechanism-Data Hybrid Method*, Mechanical Systems and Signal Processing, 224, 112041, https://doi.org/10.1016/j.ymssp.2024.112041.
[16] JEDRZEJEWSKI J., KWASNY W., 2015, *Development of Machine Tool Operational Properties*, Journal of Machine Engineering, 15/1, 5–24.
[17] CHICCO D., SICHENZE A., JURMAN G., 2025, *A Simple Guide to the Use of Student's T-Test, Mann-Whitney U Test, Chi-Squared Test, and Kruskal-Wallis Test in Biostatistics*, BioData Mining, 18/1, 56, https://doi.org/10.1186/s13040-025-00465-6.
[18] SOUSA A.R., 2018, *Metrological Evaluation of a Coordinate Measuring Machine with 5-Axis Measurement Technology*, Procedia CIRP, 75, 367–372, https://doi.org/10.1016/j.procir.2018.04.035.
[19] LI R.-J., FAN K.-C., HUANG Q.-X., ZHOU H., GONG E.-M., XIANG M., 2016, *A Long-Stroke 3D Contact Scanning Probe for Micro/Nano Coordinate Measuring Machine*, Precision Engineering, 43, 220–229, https://doi.org/10.1016/j.precisioneng.2015.08.001.